SNARE-mediated rapid lysosome fusion in membrane raft clustering and dysfunction of bovine coronary arterial endothelium

Wei-Qing Han, Min Xia, Chun Zhang, Fan Zhang, Ming Xu, Ning-Jun Li and Pin-Lan Li

Am J Physiol Heart Circ Physiol 301:H2028-H2037, 2011. First published 16 September 2011; doi:10.1152/ajpheart.00581.2011

Am J Physiol Heart Circ Physiol 301: H2028–H2037, 2011.
First published September 16, 2011; doi:10.1152/ajpheart.00581.2011.

SNARE-mediated rapid lysosome fusion in membrane raft clustering and dysfunction of bovine coronary arterial endothelium

Wei-Qing Han, Min Xia, Chun Zhang, Fan Zhang, Ming Xu, Ning-Jun Li, and Pin-Lan Li

Department of Pharmacology and Toxicology, Medical College of Virginia Campus, Virginia Commonwealth University, Richmond, Virginia

Submitted 20 June 2011; accepted in final form 6 September 2011

Han WQ, Xia M, Zhang C, Zhang F, Xu M, Li NJ, Li PL. SNARE-mediated rapid lysosome fusion in membrane raft clustering and dysfunction of bovine coronary arterial endothelium. *Am J Physiol Heart Circ Physiol* 301: H2028–H2037, 2011. First published September 16, 2011; doi:10.1152/ajpheart.00581.2011.—The present study attempted to evaluate whether soluble *N*-ethylmaleimide-sensitive factor attachment protein receptors (SNAREs) mediate lysosome fusion in response to death receptor activation and contribute to membrane raft (MR) clustering and consequent endothelial dysfunction in coronary arterial endothelial cells. By immunohistochemical analysis, vesicle-associated membrane proteins 2 (VAMP-2, vesicle-SNAREs) were found to be abundantly expressed in the endothelium of bovine coronary arteries. Direct lysosome fusion monitoring by *N*-(3-triethylammoniumpropyl)-4-[4-(dibutylamino)styryl]pyridinium dibromide (FM1-43) quenching demonstrated that the inhibition of VAMP-2 with tetanus toxin or specific small interfering ribonucleic acid (siRNA) almost completely blocked lysosome fusion to plasma membrane induced by Fas ligand (FasL), a well-known MR clustering stimulator. The involvement of SNAREs was further confirmed by an increased interaction of VAMP-2 with a target-SNARE protein syntaxin-4 after FasL stimulation in coimmunoprecipitation analysis. Also, the inhibition of VAMP-2 with tetanus toxin or VAMP-2 siRNA abolished FasL-induced MR clustering, its colocalization with a NADPH oxidase unit gp91^{phox}, and increased superoxide production. Finally, FasL-induced impairment of endothelium-dependent vasodilation was reversed by the treatment of bovine coronary arteries with tetanus toxin or VAMP-2 siRNA. VAMP-2 is critical to lysosome fusion in MR clustering, and this VAMP-2-mediated lysosome-MR signalosomes contribute to redox regulation of coronary endothelial function.

soluble *N*-ethylmaleimide-sensitive factor attachment protein; exocytosis; vesicle fusion; molecular trafficking; coronary vasorelaxation

LIPID RAFTS, now called membrane rafts (MRs) (22, 46), refer to subdomains of the plasma membrane, which were initially identified by their relative resistance to Triton X-100 extraction. Unlike the rest of the membrane, MRs are enriched in cholesterol, with saturated acyl chains such as sphingolipids and glycosphingolipids (5, 39). More and more studies showed that MRs serve as an important cellular signaling mechanism in the regulation of a variety of cell functions or activities such as cell apoptosis, cell adhesion, and cell-cell interactions (5, 26, 39). In particular, there are accumulating evidence showing that MRs were involved in the clustering of nicotinamide-adenine dinucleotide phosphate (NADPH) oxidase subunits such as gp91^{phox}, p47^{phox}, and p22^{phox}, leading to the activation of this enzyme in coronary arterial endothelial cells (CAECs) and other cells (10, 28, 38). With respect to the mechanism mediating MR clustering and associated signaling, our recent studies showed that lysosome fusion is a trigger for MR clustering to activate a series of signaling pathways in endothelial cells (ECs) in response to various death receptor ligands such as Fas ligand (FasL), tumor necrosis factor-α, and endostatin. Through lysosome fusion, acid sphingomyelinase (ASMase) on lysosome membrane was first translocated to plasma membrane and then activated there. The product of ASMase, ceramide, may initiate MR clustering, leading to the aggregation of NADPH oxidase subunits and other associated components such as *Rac*1. In such MR clusters, NADPH oxidase is activated to produce superoxide (O_2^-) and consequently results in endothelial dysfunction. This MR-mediated transmembrane signaling mechanism is considered as an early event during activation of the death receptors (19, 51). However, the mechanisms underlying lysosome fusion remains largely unknown.

Soluble *N*-ethylmaleimide-sensitive factor attachment protein receptors (SNAREs) are a superfamily of small and mostly membrane-anchored proteins that mediate membrane fusion such as lysosome exocytosis in a variety of eukaryotic cells (18, 30). The minimal machinery underlying vesicle fusion includes three SNARE proteins: one vesicle membrane protein synaptobrevin (also called vesicle-associated membrane protein, VAMP) and two plasma membrane proteins, syntaxin and soluble *N*-ethylmaleimide-sensitive factor attachment protein (SNAP)-23/25. These three proteins form a stable four-helical bundle and then lead to membrane fusion (30). Among these proteins, VAMP-2 plays a key role in the fusion and exocytosis of synaptic vesicles in neuron cells. It is also involved in regulated exocytosis in non-secretory cells, such as insulin-regulated translocation of glucose transporter-4-containing vesicles in adipocytes (27, 47), vasopressin regulated translocation of aquaporin-2-containing vesicles in renal epithelial cells (41), insulin secretion in pancreatic β-cells (36), and IL-1β exocytosis in leukocytes (6). However, there is no study showing that VAMP-2-mediated vesicle exocytosis is related to redox signaling pathway. The present study hypothesized that VAMP-2 mediates lysosome fusion in response to Fas activation and thereby contributes to MR clustering, NADPH oxidase activation, and consequent endothelial dysfunction in the coronary endothelium.

MATERIALS AND METHODS

Cell culture. Bovine CAECs were isolated and maintained in RPMI 1640 medium (Invitrogen, Carlsbad, CA) containing 10% fetal bovine serum (HyClone, Waltham, MA) and 1% antibiotics (Sigma, St. Louis, MO) as previously described (1, 19, 51). Cells were identified by staining with specific EC marker 1,1′-dioctadecyl-3–3-3′-3′-te-

Address for reprint requests and other correspondence: P.-L. Li, Dept. of Pharmacology & Toxicology, Medical College of Virginia Campus, Virginia Commonwealth Univ., 410 N. 12th, Richmond, VA, 23298 (e-mail: pli@vcu.edu).

tramethyl-in-docarbocyanine perchlorate-acetylated low-density lipoprotein (DiL-Ac-LDL). All cell studies were performed by using CAECs of two to four passages.

Immunohistochemistry. After bovine arteries were washed three times with phosphate-buffered saline (PBS) containing (in mmol/l) 137 NaCl, 2.7 KCl, 10 Na_2HPO_4, and 2 KH_2PO_4 (pH: 7.4), they were fixed with a 4% formaldehyde solution. Tissues were embedded in paraffin and were cut into transverse sections (5 μm thick). After being defatted and rehydrolated, slides were probed with anti-VAMP-2 or syntaxin-4 antibodies and then treated with corresponding secondary antibody and streptavidin-horseradish peroxidase (24).

Confocal microscopy of molecular colocalization. CAECs were fixed with 4% paraformaldehyde in PBS for 10 min. Some cells were then permeabilized with 0.5% Tween-20 for 15 min. For detection of the colocalization of lysosome-associated membrane protein (Lamp-1) with VAMP-2, the CAECs were first incubated with mouse anti-Lamp1 antibody (1: 500, Abcam, San Francisco, CA) and Alexa 488-conjugated goat anti-mouse antibody (1:500, Molecular Probes, Carlsbad, CA). After being washed with PBS, CAECs were incubated with rabbit anti-VAMP-2 antibody (1:500, Abcam) and Alexa 555-conjugated goat anti-rabbit antibody (1:500, Molecular Probes). The parameters of acquisition using objective plapo 60 × O with a focus mode of ×2, normal filter mode, confocal apepture of 2 and 2.68 s/scan.

CAECs were incubated with 8 μM *N*-(3-triethylammoniumpropyl)-4-[4-(dibutylamino)styryl]pyridinium dibromide (FM1-43, Molecular Probes) for more than 2 h. After fixation with 4% paraformaldehyde and being permeabilized with 0.5% Tween-20 for 15 min, the cells were stained with mouse anti-Lamp1 antibody (1: 500, Abcam) and Alexa 555-conjugated goat anti-mouse antibody (1:500, Molecular Probes). Some cells were treated with 8 μM FM1-43 and 150 nM Red DND-99 (Molecular Probes) and then used for confocal imaging. Manders' overlap coefficients (m1 and m2 coefficients) were used to indicate the colocalization between Lamp-1 and VAMP-2, FM1-43 and Lamp-1/Red DND-99 (53).

Inhibition of VAMP-2 with RNA interference or tetanus toxin. CAECs were transfected with VAMP-2 small interfering ribonucleic acid (siRNA) 5′-CAUCAUCGUUUACUUCAGCUCUUAA-3′ according to manufacturer's instructions (TransMessenger transfection kit, Qiagen, Valencia, CA). Scrambled siRNA was used as negative control. In some experiments, CAECs were treated with tetanus toxin (10 nmol/l, 2 h, Sigma) to cleave to VAMP-2 protein.

FM1-43 fluorescence quenching and dequenching. FM1-43 quenching and dequenching experiments were performed to detect lysosomal fusion to the cell membrane as we previously described (16, 52). For quenching experiments, after cells were loaded with 8 μmol/l FM1-43 (Molecular Probes) for 2 h, 1 mmol/l bromide phenol blue (BPB) was added in the extracellular medium. For dequenching experiments, cells were simultaneously loaded with 8 μmol/l FM1-43 and 1 mmol/l BPB for 2 h. After the CAECs were loaded by different dyes or their combinations and then washed with fetal bovine serum free medium, FM1-43 fluorescence was monitored under confocal microscopy (Olympus) with a low power (λ excitation = 488 nm) of laser. The fluorescence puncta were chosen based on the brightness of staining close to cell membrane after loading of FM1-43. In this way, we could select most focused lysosomes and continuously monitor fluorescence changes before and after FasL stimulation. In quenching configuration, FM1-43 fluorescence decreases because of BPB entering the cells and quenches FM1-43 after lysosome fusion upon FasL stimulation. Therefore, the detection of FM1-43 fluorescence quenching by BPB in bath solution indicates lysosome fusion to the cell membrane. The rationale for dequenching experiments is that when lysosomes are fused with the cell membrane under FasL stimulation, FM1-43 fluorescence tends to increase because BPB, which FM1-43 fluorescence, may flow out of lysosomes much easier compared with FM1-43.

Confocal analysis of MR clusters and its colocalization with gp91^{phox} or VAMP-2. Detection of MR clusters was performed as we previously described (20, 50). In brief, GM1 gangliosides enriched in MRs were stained by Alexa 488-labeled cholera toxin B (1 μg/ml, 2 h, Molecular Probes). Clustering was defined as one or several intense spots or patches, rather than diffuse fluorescence on the cell surface, whereas a vast majority of unstimulated cells displayed a homogeneous distribution of fluorescence throughout the membrane. In each experiment, the presence or absence of clustering in samples was independently scored by unwitting researchers after specifying the criteria for positive spots of fluorescence. Cells displaying a homogeneous distribution of fluorescence were marked negative. Results were given as the percentage of cells showing one or more clusters after the indicated treatment.

For dual-staining detection of the colocalization of MRs and NADPH oxidase subunits, gp91^{phox} or VAMP-2, CAECs were further incubated with mouse anti-gp91^{phox} monoclonal antibody (1:250; BD Biosciences, San Jose, CA) or rabbit anti-VAMP-2 polyclonal antibodies (Abcam, 1:500) separately, which was followed by Alexa 555-conjugated anti-mouse or anti-rabbit secondary antibody (Molecular Probes, Carlsbad, CA) as needed, respectively. Staining was visualized through sequentially scanning on an Olympus scanning confocal microscope (Olympus, Tokyo, Japan). Colocalization was analyzed by Image Pro Plus software, and the colocalization coefficient was represented by Pearson's correlation coefficient (54).

Fluorescence resonance energy transfer assay. Fluorescein isothiocyanate/tetramethylrhodaminoisothiocyanate (FITC/TRITC) pairs were used for fluorescence resonance energy transfer (FRET) assay of MRs with VAMP-2. VAMP-2 antibody was labeled with FITC by using a labeling kit (Invitrogen, Carlsbad, CA) according to manual instruction. CAECs were stained with FITC-conjugated anti-VAMP-2 antibody and TRITC-conjugated cholera toxin B (2 μg/ml, 2 h, List labs, Campbell, CA). FasL at 10 ng/ml was used to stimulate cells for 20 min. Alexa 488/Alexa 555 pairs were used for FRET assay of Lamp-1 and VAMP-2/ASMase. Mouse Lamp-1 primary antibody and rabbit ASMase primary antibody were labeled with Alexa 488 and Alexa 555 by using a labeling kit (Invitrogen, Carlsbad, CA) according to manual instruction, respectively. CAECs were first stained with Alexa 488-conjugated anti-Lamp-1 antibody and then stained with Alexa 555-conjugated anti-VAMP-2 antibody or Alexa 555-conjugated anti-ASMase antibody. After the prebleaching image was normally taken, the laser intensity at the excitement wavelength of the acceptor (TRITC) was increased from 50 to 98% and continued to excite the cell sample for 2 min to bleach the acceptor fluorescence. After the intensity of the excitement laser for acceptor was adjusted back to 50%, the postbleaching image was taken for FITC. A FRET image was obtained by subtraction of the prebleaching images from the postbleaching images and given a dark blue color. After the FITC fluorescence intensities of the pre-, post-, and FRET images were measured, the FRET efficiency was calculated through the following equation: $E = (FITC_{post} - FITC_{pre})/FITC_{post} \times 100\%$ (19).

SNARE complex formation and coimmunoprecipitation assay. The measurement of SNARE complex formation was performed as previously reported (9, 43). After cells were treated with FasL (10 ng/ml, 20 min), cell proteins were collected and duplicate samples were either boiled for 10 min to dissociate the complex or incubated at 30°C for 5 min and then used for immunoblotting.

The interaction between VAMP-2 and syntaxin-4 was examined with a coimmunoprecipitation kit (Pierce Biotechnology, Rockford, IL) according to the manufacturer's instructions. In brief, a rabbit anti-VAMP-2 antibody (Abcam) was first immobilized on the coupling gel beads and then incubated with membrane protein for 2 h. After being eluted and regenerated, the immunocomplexes were inactivated and prepared for SDS-PAGE, immunoblotting to VAMP-2 and syntaxin-4 was performed, respectively.

Flotation of membrane lipid microdomains. The translocation of VAMP-2 and syntaxin-4 in caveolar and noncaveolar domain was

detected by using a nondetergent four-layer flotation as previously described (49). Confluent CAECs were washed with PBS, scraped into isotonic buffer containing (in mmol/l) 250 sucrose, 20 Tris·HCl, 1 EDTA, 15 KCl, 2 $MgCl_2$, and 1 PMSF and 2 ml/ml protease inhibitors cocktail (pH 7.5) and were homogenized by five passages through a 25-gauge needle. The cell lysate was centrifuged at 10,000 *g* for 45 min at 4°C, and the membrane pellet was resuspended in the same isotonic buffer. The plasma membrane was isolated by loading the resuspended membrane pellet onto a 1.12 mol/l sucrose cushion and centrifuging at 100,000 *g* for 2 h. The plasma membrane fraction at the interface was collected, diluted with PBS, and pelleted by centrifugation at 200,000 *g* for 1 h. Three milliliters of 35% sucrose solution, 4 ml of 21% sucrose solution, and 1 ml of 5% sucrose solution were overlaid on 4 ml of extraction mixture. The gradient was formed in a 14 × 89-mm Beckman centrifuge tube and centrifuged at 180,000 *g* for 20 h in a SW41 rotor (Beckman) at 4°C. Fractions were collected from the top of the sucrose gradient.

Flowcytometric analysis of ASMase translocation onto plasma membrane. The ASMase level on the plasma membrane was assessed with flow cytometry as previously described (45). CAECs were harvested and washed with PBS and then blocked with 1% BSA for 10 min at 4°C. After two washes, the pellet was added to 100 ml PBS and incubated with ASMase primary antibody (1:200; Santa Cruz Biotechnology), followed by incubation with Alexa 555-labeled anti-rabbit secondary antibody (1: 500; Molecular Probes). Stained cells were run on a Guava Easycyte Mini Flow Cytometry System (Guava Technologies, Hayward, CA) and analyzed with Guava acquisition and analysis software (Guava Technologies).

Electron spin resonance detection of endothelial O_2^-. Electron spin resonance was performed as we previously described (51). Gently collected CAECs were suspended in modified Krebs-HEPES buffer containing (in mmol/l) 99.01 NaCl, 4.69 KCl, 1.87 $CaCl_2$, 1.20 $MgSO_4$, 1.03 K_2HPO_4, 25.0 $NaHCO_3$, 20.0 Na-HEPES, and 11.1 glucose (pH 7.4), supplemented with deferoxamine (100 μmol/l; metal chelator). Approximately 1×10^6 cells were then incubated with FasL (10 ng/ml) for 15 min; these cells were subsequently mixed with 1 mmol/l of the O_2^--specific spin trap 1-hydroxy-3-methoxycarbonyl-2,2,5,5-tetramethylpyrrolidine (CMH) in the presence or absence of manganese-dependent superoxide dismutase (500 U/ml, Sigma). The cell mixture was then loaded in glass capillaries and immediately kinetically analyzed for O_2^- production for 10 min. The superoxide dismutase-inhibitable fraction of the signal was compared. The electron spin resonance settings were as follows: biofield, 3,350; field sweep, 60 G; microwave frequency, 9.78 GHz; microwave power, 20 mW; modulation amplitude, 3 G; 4,096 points of resolution; receiver gain, 100; and kinetic time, 10 min.

Endothelium-dependent vasodilation in isolated small coronary artery. Fresh bovine hearts were obtained from a local abattoir. Small coronary arteries (~200 μm ID) were mounted in a Multi Myograph 610M (DMT, Aarhus, Denmark) for isometric tension recording (4). The vasodilatory curves to bradykinin (BK, a vasodilating peptide) were obtained after arteries were precontracted with 9,11-dideoxy-11α,9α-epoxymethanoprostaglandin $F_{2\alpha}$ (U-46619, thromboxane receptor agonist, 50 nmol/l, Sigma) with or without FasL (10 ng/ml, 20 min), tetanus toxin (10 nmol/l, 2 h) treatment. For some arteries, the ultrasound microbubble technology was used to transfect endothelium-intact arteries with scrambled small RNA or VAMP-2 siRNA as previously described (23).

Statistics. Data are presented as means ± SE. Significant differences between and within multiple groups were examined using ANOVA for repeated measures, followed by Duncan's multiple-range

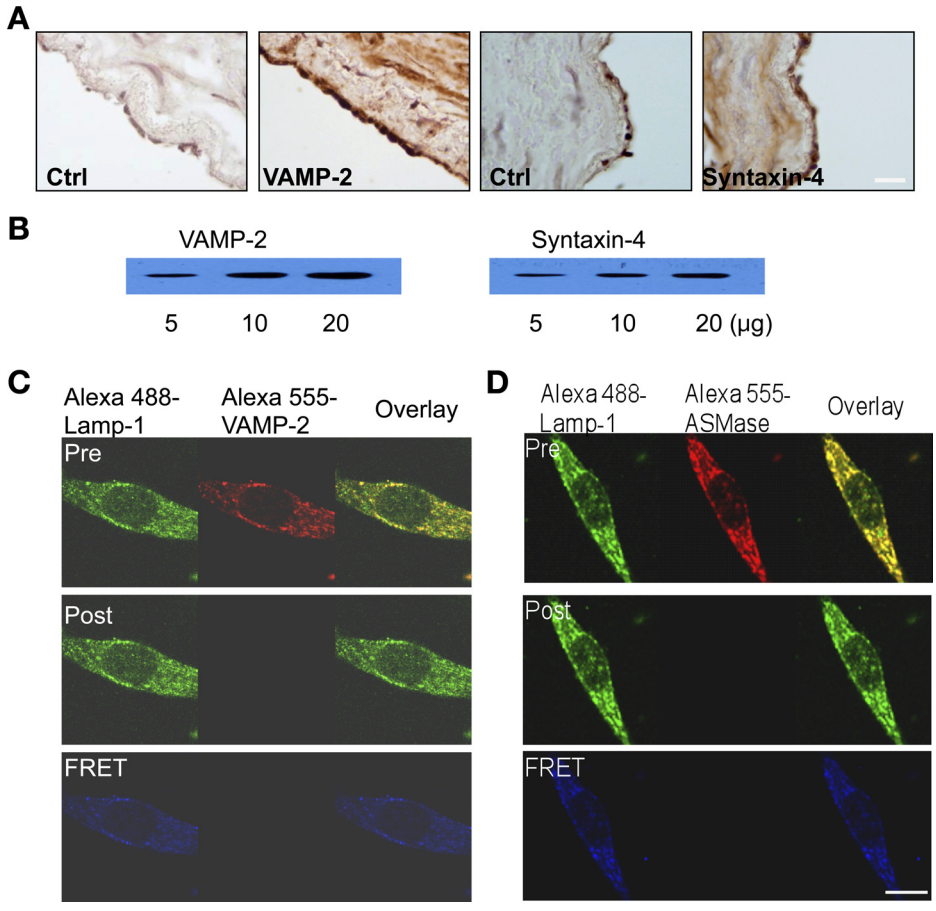

Fig. 1. *A*: immunohistochemistry of vesicle-associated membrane proteins 2 (VAMP-2) and syntaxin-4 in bovine coronary artery. *B*: detection of VAMP-2 and syntaxin-4 expression in bovine coronary arterial endothelial cells (CAECs) by using 5, 10, and 20 μg proteins for immunoblotting assay. *C*: fluorescence resonance energy transfer (FRET) assay between VAMP-2 and lysosome marker lysosome-associated membrane protein (Lamp-1). Permeabilized CAECs were stained with Alexa 488-coupled Lamp-1 antibody and Alexa 555-coupled VAMP-2 antibody, respectively, and then used for confocal microscopy assay. *D*: FRET assay between ASMase and lysosome marker Lamp-1. Permeabilized CAECs were stained with Alexa 488-coupled Lamp-1 antibody and Alexa 555-coupled ASMase antibody, respectively, and then used for confocal microscopy assay. Ctrl, control. Scale bar, 50 μm in *A* and 10 μm in *D*.

test. A Student's *t*-test was used to detect significant differences between two groups. $P < 0.05$ was considered statistically significant.

RESULTS

Colocalization between VAMP-2 and Lamp-1. Immunohistochemistry with bovine coronary arteries showed that the endothelial layer exhibited strong VAMP-2 and syntaxin-4 staining compared with control, whereas the medial layer was only slightly stained (Fig. 1*A*). Western blot analysis assay with VAMP-2 and syntaxin-4 antibody showed 19- and 33-kDa bands corresponding to their specific molecular mass, respectively (Fig. 1*B*). Figure 1*C* showed that VAMP-2 showed strong FRET with a specific lysosome marker, Lamp-1, in permeabilized cells (10.5 ± 1.75, $n = 4$). ASMase was also found to be located on lysosome membrane as the strong FRET efficiency (17.8 ± 1.0, $n = 6$) between ASMase and Lamp-1 in permeabilized CAECs (Fig. 1*D*). These results indicated that VAMP-2 and ASMase were mainly located on lysosome membrane in CAECs.

VAMP-2 inhibition attenuated FasL-induced lysosome fusion. The possible contribution of VAMP-2 to lysosome fusion was determined by FM1-43 quenching and dequenching. As shown in Fig. 2*A*, FM1-43 showed strong colocalization with lysoTracker Red DND-99 (colocalization coefficient with FM1-43: 85.9 ± 2.80%), indicating that FM1-43 specifically labeled lysosomes after CAECs were loaded with this dye for 2 h. The decrease in FM1-43 fluorescence (quenching) indicates lysosome fusion. This is because BPB as a quenching substance in the both solutions enters cell lysosomes, where it acts to quench FM1-43. If lysosomes are not fused into the cell membrane, the BPB may not enter the lysosome containing FM1-43, and therefore no quenching will occur and fluorescence will remain unchanged. For dequenching experiments, lysosomes of CAECs were loaded simultaneously with 8 μM FM1-43 and 1 mM BPB for 2 h and then underwent different treatments. After lysosomes are fused with the cell membrane under FasL stimulation, FM1-43 fluorescence tends to increase because BPB may flow out of the lysosome much easier compared with FM1-43 and then dissociate with FM1-43. Therefore, the detection of FM1-43 fluorescence dequenching also indicates lysosomal fusion. Figure 2*B* showed that VAMP-2 siRNA or tetanus toxin significantly decreased VAMP-2 protein content in Western blot analysis, and both treatments almost completely blocked FasL-induced quench-

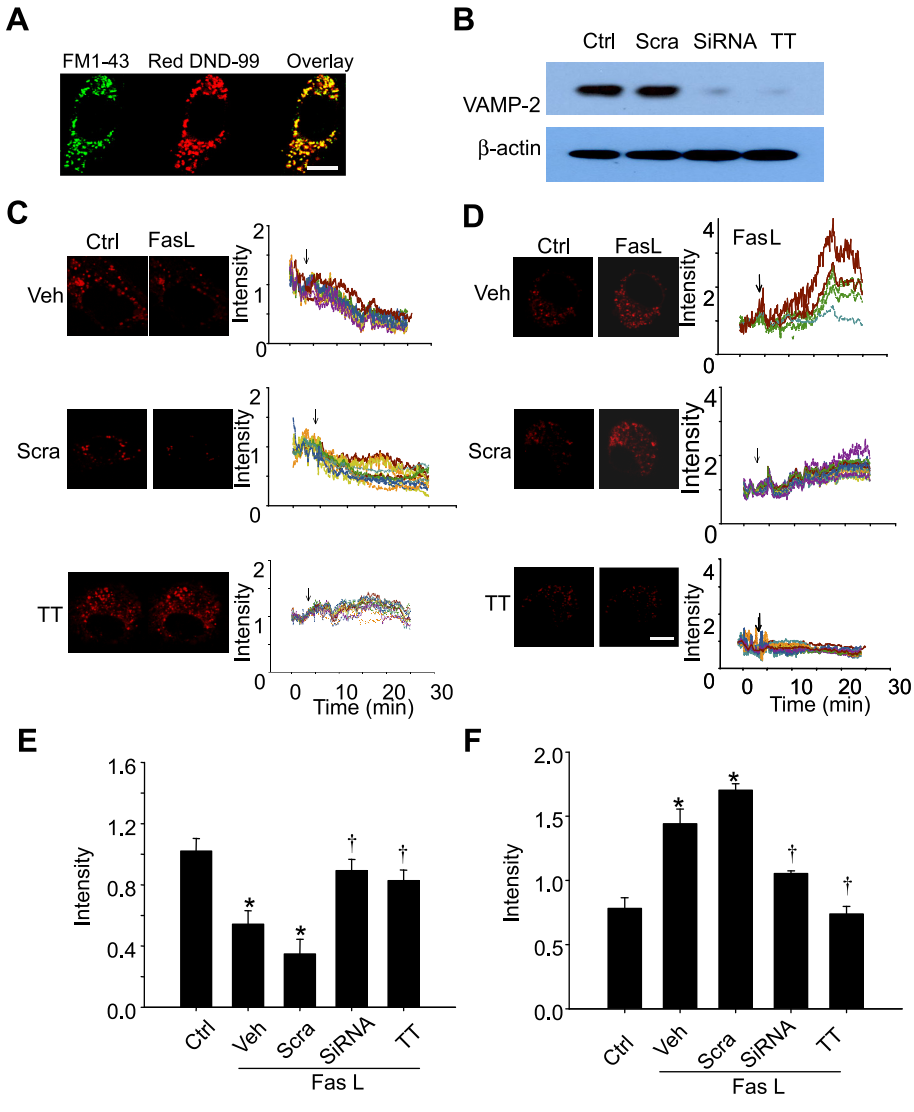

Fig. 2. *A*: colocalization of *N*-(3-triethylammoniumpropyl)-4-[4-(dibutylamino)styryl]pyridinium dibromide (FM1-43) with lysoTracker Red DND-99 detected by confocal microscopy in CAECs. *B*: inhibitory effect of VAMP-2 small interfering RNA (siRNA) and tetanus toxin (TT) on VAMP-2 level in CAECs in Western blot assay. β-Actin was used as a loading control. Representative (*C* and *D*) and summarized (*E* and *F*) data show the inhibitory effect of VAMP-2 siRNA and TT on FasL-induced FM1-43 fluorescence quenching (*C* and *E*) and dequenching (*D* and *F*) in CAECs. Arrows indicate beginning of treatments. Fluorescence after treatment was normalized by that before treatment ($n = 80$ puncta from 6 batches of cells). *$P < 0.05$ vs. control group; †$P < 0.05$ vs. vehicle (Veh) group. Scra, scrambled RNA; FasL, Fas ligand. Scale bar, 10 μm in *A* and *D*.

ing (Fig. 2, *C* and *E*) and dequenching (Fig. 2, *D* and *F*), indicating that VAMP-2 plays an important role in FasL-induced lysosome fusion. In contrast, there was no detectable VAMP-3 (another SNARE protein, data not shown) signaling in CAECs, suggesting a specific role of VAMP-2 in CAECs.

Our previous studies showed that the accumulation of ASMase on plasma membrane and its activation play a critical role in MR clustering. We then examined whether VAMP-2 inhibition would affect such translocation of ASMase. The percentage of cells with ASM was significantly increased after FasL treatment in flowcytometry assay, and this was significantly prevented by the prior treatment with VAMP-2 siRNA or tetanus toxin (data not shown).

SNARE complex formation and interaction between VAMP-2 and syntaxin-4. Biochemical analysis was next performed to examine whether FasL induces SNARE complex formation. When cell lysates were immunoblotted with VAMP-2 antibody, an 85-kDa band was detected besides a 19-kDa VAMP-2 band (Fig. 3*A*). This 85-kDa band, corresponding to the size of SNAREs complex, was stable at 30°C but was dissociated after boiling. Summarized data showed that FasL significantly increased this 85-kDa band (control, 1.0 ± 0.0 vs. FasL treatment, 1.33 ± 0.07; results were normalized to β-actin. $P < 0.05$, $n = 4$ batches of cells).

To further examine whether this vesicle-SNARE protein (VAMP-2) interacts with other SNARE complex unit, we performed coimmunoprecipitation assay. The cell lysates were first coimmunoprecipitated with VAMP-2 antibody, and elutes were then immunoblotted with anti-VAMP-2 and syntaxin-4 antibodies, respectively. As shown in Fig. 3*B*, there was no difference in the total VAMP-2 and syntaxin-4 abundance in control and FasL-treated samples before coimmunoprecipitation treatment. After coimmunoprecipitation, there was also no difference in VAMP-2 abundance between control and FasL-treated samples. In contrast, syntaxin-4 was significantly increased in FasL-treated samples, suggesting that their interaction was increased.

FRET between MRs and VAMP-2. We then determined whether SNAREs-mediated lysosome fusion contributes to MR clustering in response to FasL stimulation. Figure 4*A* shows that MRs were distributed over the EC membranes by weak diffused green fluorescence under resting conditions. After FasL stimulation, green fluorescent patches were formed on the CAEC membranes, and this effect was prevented by the presence of tetanus toxin or VAMP-2 siRNA. In Fig. 4*B*, fluorescent images made under prebleaching condition showed that in control CAECs, FRET image showed that there was very low FRET detected. After FasL stimulation, however, a remarkably increased FRET intensity was observed (Fig. 4, *B* and *C*). Figure 4*D* shows that Fas-associated death domain was not clustered after FasL treatment (control, 21.5 ± 1.85, and FasL, 19.1 ± 3.14, $P > 0.05$), indicating that apoptosis-related signaling pathway may not be involved.

Translocation of SNAREs component from caveolin to noncaveolin domain. A modified nondetergent four-layer flotation was also performed to examine the distribution of VAMP-2 and syntaxin-4. As shown in Fig. 5, membrane MRs were fractionated into 5–21% and 21–35% sucrose interfaces, corresponding to noncaveolar and caveolar domains, respectively. VAMP-2 and syntaxin-4 were mostly located in caveolar domains in control cells. After FasL stimulation, both VAMP-2 and syntaxin-4 were mostly transferred to noncaveolar domains.

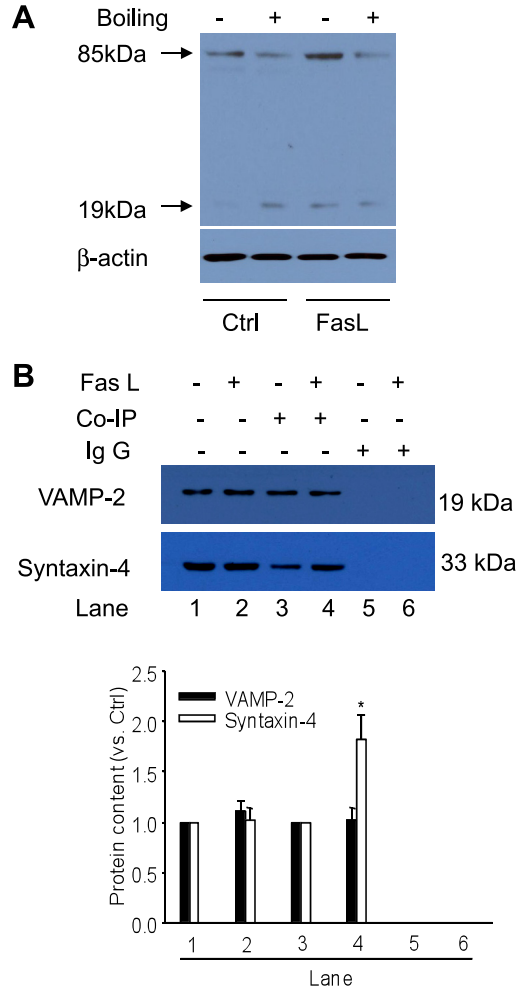

Fig. 3. A: FasL increased soluble *N*-ethylmaleimide-sensitive factor attachment protein receptors (SNAREs) complexes formation in bovine CAECs. *Lanes 1* and *2* (without and with boiling) were from control samples, and *lanes 3* and *4* (without and with boiling) were from FasL-treated samples. The 85-kDa band in *lanes 1* and *3* without boiling was calculated to indicate SNARE complex. β-Actin was used as a loading control. *B*: the precipitates trapped with anti-VAMP-2 antibody in control and FasL-treated CAECs were immunoblotted with anti-syntaxin-4 antibody and then reprobed with anti-VAMP-2 antibody (*lanes 3* and *4*). The samples without undergoing coimmunoprecipitation (Co-IP) were used as loading control (*lanes 1* and *2*); unspecific IgG was used for Co-IP to validate the specificity of this method (*lanes 5* and *6*). Summarized data show the effects of FasL on syntaxin-4 and VAMP-2 in different treatments ($n = 4$ batches of cells). *$P < 0.05$ vs. control group.

VAMP-2 inhibition reversed FasL-induced gp91^{phox} clustering and O_2^- production. We next examined whether this VAMP-2-mediated lysosome fusion and MR clustering were involved in FasL-induced NADPH oxidase subunit clustering and its activation because MR clustering is closely associated with the formation of redox signaling platforms. As shown in Fig. 6, FasL induced significant clustering of gp91^{phox}, which was significantly prevented by VAMP-2 siRNA or tetanus toxin. Similarly, FasL markedly increased O_2^- production as indicated by electron spin resonance spectra assay, and this effect was almost fully blocked by tetanus toxin or VAMP-2 siRNA (Fig. 7, *A* and *B*).

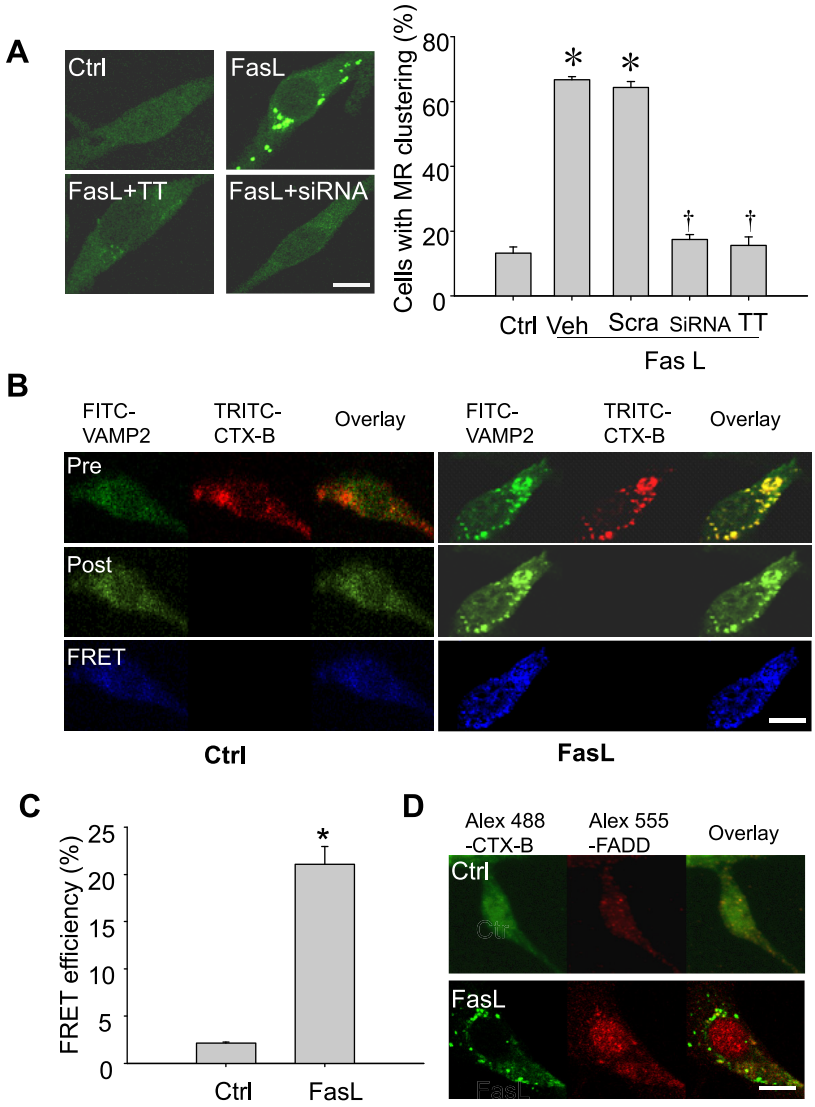

Fig. 4. *A*: effects of VAMP-2 siRNA and TT on FasL-induced membrane raft (MR) formation in CAECs. Representative image (*B*) and bar graph (*C*) show the effect of FasL on FRET efficiency between FITC-VAMP-2 and tetramethylrhodamin-oisothiocyanate-cholera toxin B (TRITC-CTXB) in CAECs. *D*: representative image showing the colocalization between MRs and Fas-associated death domain (FADD) detected by confocal microscopy in CAECs with or without FasL treatment. Scale bar, 10 μm in *A*, *B*, and *D*; $n = \sim 5$ to 6 batches of cells. $^*P < 0.05$ vs. control group; $\dagger P < 0.05$ vs. vehicle group.

VAMP-2 inhibition reversed FasL-induced impairment of endothelium-dependent vasodilation. Finally, the involvement of VAMP-2 in FasL-induced impairment of vasodilation was examined. As shown in Fig. 7*C*, BK produced a concentration-dependent relaxation in endothelium-intact bovine coronary arterial rings. When the arteries were incubated with FasL, the BK-induced vasodilator response was blunted. As expected, the incubation with tetanus toxin or VAMP-2 siRNA prevented the damage effect of FasL, indicating that VAMP-2 was involved in FasL-induced impaired vasodilation. In contrast, VAMP-2 siRNA treatment did not affect vascular contraction (force generation) compared with scramble RNA treatment: scrambled RNA group with 1.98 ± 0.02 g vs. siRNA group with 2.16 ± 0.09 g, $P > 0.05$. These results indicate that VAMP-2 siRNA treatment might have no significant effect on smooth muscle contraction ability in our vessel preparations and that the effect on the endothelium-dependent vasodilation was caused by corresponding changes in ECs.

DISCUSSION

In the present study, we addressed the role of SNAREs in FasL-induced lysosome fusion, MR clustering, and endothelial dysfunction. It was found that VAMP-2 is located on lysosomes of ECs and its inhibition by tetanus toxin or siRNA attenuated lysosome fusion and almost fully abolished FasL-induced MR clustering, increased O_2^- production, and impairment of vasodilation.

VAMP-2, a prototype SNARE protein, was found to be abundant in the coronary arterial endothelium in immunohistochemistry analysis, which is consistent with previous studies showing this SNAREs protein was present in ECs (11, 12, 29). VAMP-2 showed high FRET efficiency with a lysosome marker Lamp-1, suggesting that VAMP-2 is present on lysosomes of CAECs. FM1-43 quenching has been used as a new method for the investigation of lysosome fusion (19, 52), which was consistent with the present study that FM1-43 was strongly colocalized with lysosome marker lysoTracker Red DND-99. The finding that VAMP-2 inhibition almost fully abolished FasL-induced FM1-43 quenching and dequenching suggests that this protein is involved in FasL-induced lysosome fusion.

Further biochemical analysis showed that FasL significantly increased a heat-sensitive 85-kDa band content, corresponding to SNAREs complex, when cell lysates without boiling were

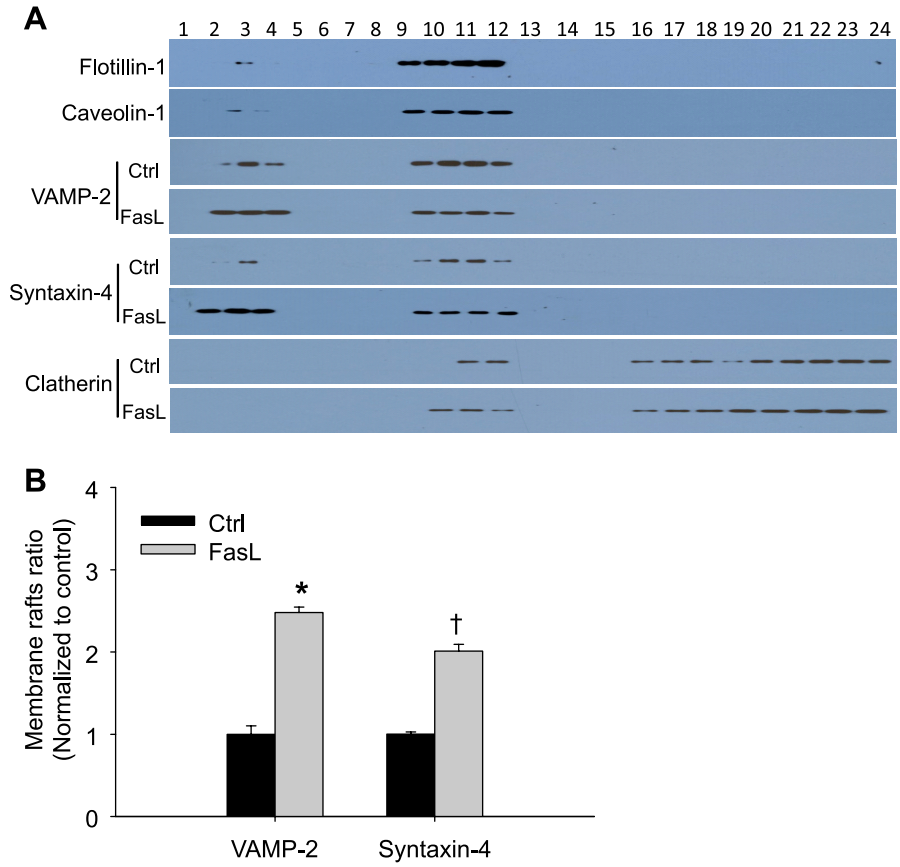

Fig. 5. Representative (*A*) and summarized (*B*) data showing the effects of FasL on VAMP-2 and syntaxin-4 distribution in different membrane fractions with 4-layer flotation. Flotillin-1 is a marker for a lipid microdomain structure protein, caveolin-1 is a caveolae domain marker, and clatherin plays a role in the formation of coated vesicles being a nonlipid raft protein. *$P < 0.05$ and †$P < 0.05$ vs. control group in VAMP-2 and syntaxin-4 groups, respectively.

immunoblotted with anti-VAMP-2 antibody (17). This SNAREs assembly was thought to proceed down a steep energy gradient and thereby force the membranes to fusion, a critical step for SNAREs-mediated vesicle fusion (2, 9, 34). Western blot analysis shows that there is no VAMP-3 expression in CAECs, indicating that other SNAREs may not be involved in lysosome fusion and the downstream signaling pathway. Coimmunoprecipitation assay showed that FasL significantly increased the interaction of VAMP-2 with a target (t)-SNARE protein syntaxin-4. Although there are several different subtypes of t-SNAREs, the involvement of syntaxin-4 in vesicle fusion has been reported in ECs, in particular, its role in the fusion of caveolae with the target plasma membrane (35). In human lung microvascular ECs, syntaxin-4 was found to participate in Weibel-Palade bodies exocytosis induced by thrombin (12). In human umbilical vein ECs and human aortic ECs, SNAREs were involved in vesicle and granule exocytosis (48). Although both VAMP-2 and syntaxin 4 were slightly expressed in the medial layer, they may not be involved in vascular contraction/relaxation since the vascular rings developed similar vascular contraction in scramble RNA and VAMP-2 siRNA-treated vascular rings (scramble, 1.98 ± 0.02 g; siRNA, 2.16 ± 0.09, $P > 0.05$), although it has been shown that VAMP-2 mediated cyclophilin A release in vascular smooth muscle cells (40).

The involvement of VAMP-2 in MR cluster was confirmed by the findings of increased FRET between MRs and VAMP-2 in FasL-treated cells, which may be caused by the translocation of VAMP-2 from lysosome membrane to plasma membrane. It has been shown that VAMP-2 was translocated from Glut-4-containing vesicles to the plasma membrane in response to insulin stimulation (42). In pancreatic β-cells, VAMP-2 was translocated from lysosomes to plasma membrane after insulin stimulation (32). These results indicate that VAMP-2 may be in a mobile phase, where it is translocated between plasma membrane and vesicle membrane, and is involved in corresponding signaling transduction. Also, it has been shown that SNAREs are located in the MR domain by flotation and that SNAREs were involved in regulated exocytosis (7). The present findings may provide new evidence that VAMP-2 and syntaxin-4 were translocated from caveolar to noncaveolar domains after FasL stimulation by using a modified four-layer flotation. Indeed, the active noncaveolar domains were found to be involved in various signaling pathways. In unstimulated cells, epidermal growth factor (EGF) receptors are concentrated in plasma membrane caveolae, and they move out of caveolae following stimulation (13, 31). In smooth muscle cells, a small heat shock protein 27 can be dephosphorylated by protein phosphatase 2A in noncaveolar domains (3).

Driven by lysosome fusion, ASMase on lysosome membrane was translocated to plasma membrane in response to FasL stimulation and then activated there (8, 15, 19, 44, 51). This is consistent with a recent study showing that ASMase is activated through translocation from intracellular compartments to the plasma membrane in an exocytic pathway requiring the t-SNARE protein syntaxin 4 (33). The early product of AMSase ceramide may act as kindling to activate lysosome trafficking and fusion with cell membrane, resulting in the production of bonfire ceramide, which then triggers MR clustering (8, 15, 19, 44, 51). Accordingly, lysosome function was

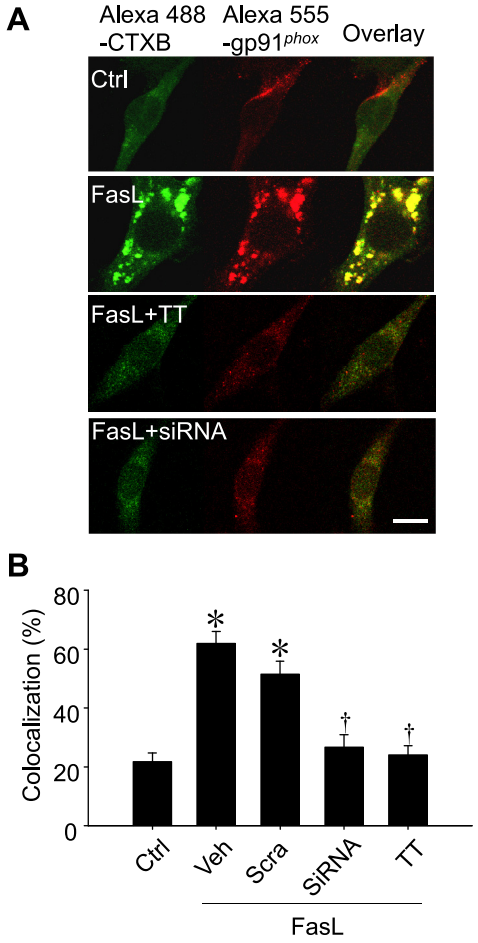

Fig. 6. Effects of VAMP-2 siRNA and TT on colocalization between MRs and gp91^{phox}. *A*: representative confocal fluorescence images for colocalization of MRs and gp91^{phox} with or without VAMP-2 siRNA and TT treatment before FasL stimulation. *B*: summarized bar graph showing the colocalization between MRs and gp91^{phox} in different treatments. Scale bar, 10 μm in *A*; n = ~5 to 6 batches of cells. *$P < 0.05$ vs. control group; †$P < 0.05$ vs. vehicle group.

found to play a critical role since FasL-induced MR clustering, subsequent O_2^- production, and impairment of vasodilation were significantly blocked by interruption of lysosome function with bafilomycin A1 and methyl-b-cyclodextrin (19) or inhibition of ASMase with specific siRNA (25, 50). As expected, the blockade of lysosome fusion with VAMP-2 inhibition in the present study abolished FasL-induced downstream signaling pathway including ASMase translocation onto plasma membrane and subsequent MR formation, gp91^{phox} clustering, and increased O_2^- production, in which the NADPH oxidase subunits were clustered together to be activated (14, 21, 37, 51). The involvement of VAMP-2 in MR-redox signaling pathway was further confirmed by the finding that its inhibition with tetanus toxin or specific siRNA or inhibition of NADPH oxidase with a specific inhibitor apocynin blocked FasL-induced impairment of vasodilation in the present and previous studies (25, 51). The involvement of vascular smooth muscle cells may be excluded since VAMP-2 siRNA did not affect vascular tension. Finally, the effect of FasL on MR cluster and redox signaling is considered as an early effect of death receptor and apoptosis may not be involved (19, 51), which is consistent with the present finding that Fas-associated death domain was not involved in MR cluster.

Although the present study validated the involvement of SNAREs, further study is needed to explore the mechanisms underlying SNAREs activation, lysosome fusion-related trafficking/tethering, and interactions of SNAREs with their partners. With a consideration of its crucial role in various types of cells, VAMP-2 may not be a target for intervention or diagnosis, although this SNARE protein indeed participates in the regulation of coronary endothelial function.

In conclusion, the present study demonstrated that VAMP-2 and syntaxin-4 formed a reactive complex in coronary ECs in response to Fas activation. This SNARE complex mediated

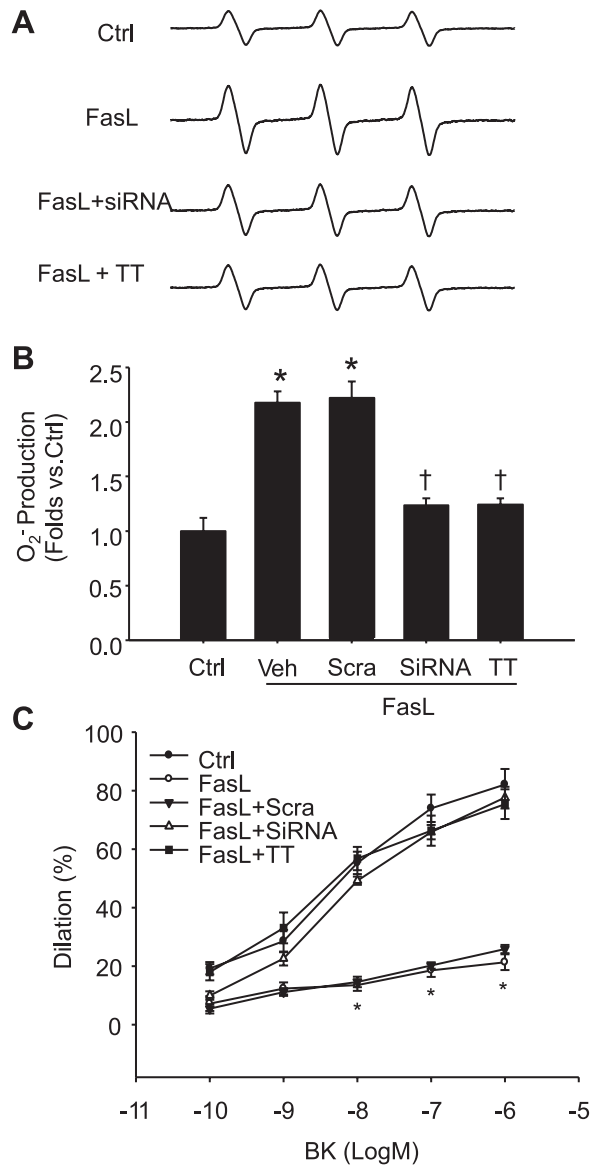

Fig. 7. A, Representative electron spin resonance spectrograph showing the inhibitory effect of VAMP-2 siRNA and TT on FasL-induced superoxide (O_2^-) production in CAECs. *B*: summarized data depicting changes in O_2^- production in CAECs in different treatments; n = ~4–6 batches of cells. *$P < 0.05$ vs. control group; †$P < 0.05$ vs. vehicle group. *C*: VAMP-2 siRNA, TT blocked FasL-induced (10 ng/ml for 20 min) damage of vasodilator response; n = 5 cow hearts. BK, bradykinin. *$P < 0.05$ vs. control, FasL + TT, or FasL + VAMP-2 siRNA.

lysosome fusion to the plasma membrane and thereby contributed to MR clustering, NADPH oxidase activation, and endothelial dysfunction. This novel transmembrane signaling mechanism may contribute to the regulation of endothelial function under different physiological and pathological conditions.

GRANTS

This study was supported by National Heart, Lung, and Blood Institute Grants HL-57244, HL-75316, and HL-091464.

DISCLOSURES

No conflicts of interest, financial or otherwise, are declared by the author(s).

AUTHOR CONTRIBUTIONS

Author contributions: W.-Q.H., M. Xia, C.Z., F.Z., and M. Xu performed experiments; W.-Q.H., M. Xia, C.Z., F.Z., M. Xu, and P.-L.L. analyzed data; W.-Q.H., M. Xia, C.Z., F.Z., M. Xu, and P.-L.L. interpreted results of experiments; W.-Q.H., M. Xia, and P.-L.L. prepared figures; W.-Q.H. and P.-L.L. drafted manuscript; W.-Q.H., N.-J.L., and P.-L.L. edited and revised manuscript; N.-J.L. and P.-L.L. conception and design of research; P.-L.L. approved final version of manuscript.

REFERENCES

1. **Bao JX, Xia M, Poklis JL, Han WQ, Brimson C, Li PL.** Triggering role of acid sphingomyelinase in endothelial lysosome-membrane fusion and dysfunction in coronary arteries. *Am J Physiol Heart Circ Physiol* 298: H992–H1002, 2010.
2. **Barszczewski M, Chua JJ, Stein A, Winter U, Heintzmann R, Zilly FE, Fasshauer D, Lang T, Jahn R.** A novel site of action for alpha-SNAP in the SNARE conformational cycle controlling membrane fusion. *Mol Biol Cell* 19: 776–784, 2008.
3. **Berrou E, Bryckaert M.** Recruitment of protein phosphatase 2A to dorsal ruffles by platelet-derived growth factor in smooth muscle cells: dephosphorylation of Hsp27. *Exp Cell Res* 315: 836–848, 2009.
4. **Brandin L, Bergstrom G, Manhem K, Gustafsson H.** Oestrogen modulates vascular adrenergic reactivity of the spontaneously hypertensive rat. *J Hypertens* 21: 1695–1702, 2003.
5. **Brown DA, London E.** Functions of lipid rafts in biological membranes. *Annu Rev Cell Dev Biol* 14: 111–136, 1998.
6. **Chai Y, Huang X, Cong B, Liu S, Chen K, Li G, Gaisano HY.** Involvement of VAMP-2 in exocytosis of IL-1 beta in turbot (*Scophthalmus maximus*) leukocytes after *Vibrio anguillarum* infection. *Biochem Biophys Res Commun* 342: 509–513, 2006.
7. **Chamberlain LH, Gould GW.** The vesicle- and target-SNARE proteins that mediate Glut4 vesicle fusion are localized in detergent-insoluble lipid rafts present on distinct intracellular membranes. *J Biol Chem* 277: 49750–49754, 2002.
8. **Cremesti AE, Goni FM, Kolesnick R.** Role of sphingomyelinase and ceramide in modulating rafts: do biophysical properties determine biologic outcome? *FEBS Lett* 531: 47–53, 2002.
9. **Di Stasi AM, Mallozzi C, Macchia G, Maura G, Petrucci TC, Minetti M.** Peroxynitrite affects exocytosis and SNARE complex formation and induces tyrosine nitration of synaptic proteins. *J Neurochem* 82: 420–429, 2002.
10. **Eum SY, Andras I, Hennig B, Toborek M.** NADPH oxidase and lipid raft-associated redox signaling are required for PCB153-induced upregulation of cell adhesion molecules in human brain endothelial cells. *Toxicol Appl Pharmacol* 240: 299–305, 2009.
11. **Feng D, Flaumenhaft R, Bandeira-Melo C, Weller P, Dvorak A.** Ultrastructural localization of vesicle-associated membrane protein(s) to specialized membrane structures in human pericytes, vascular smooth muscle cells, endothelial cells, neutrophils, and eosinophils. *J Histochem Cytochem* 49: 293–304, 2001.
12. **Fu J, Naren AP, Gao X, Ahmmed GU, Malik AB.** Protease-activated receptor-1 activation of endothelial cells induces protein kinase Calpha-dependent phosphorylation of syntaxin 4 and Munc18c: role in signaling p-selectin expression. *J Biol Chem* 280: 3178–3184, 2005.
13. **Furuchi T, Anderson RG.** Cholesterol depletion of caveolae causes hyperactivation of extracellular signal-related kinase (ERK). *J Biol Chem* 273: 21099–21104, 1998.
14. **Groemping Y, Rittinger K.** Activation and assembly of the NADPH oxidase: a structural perspective. *Biochem J* 386: 401–416, 2005.
15. **Gulbins E, Li PL.** Physiological and pathophysiological aspects of ceramide. *Am J Physiol Regul Integr Comp Physiol* 290: R11–R26, 2006.
16. **Harata NC, Choi S, Pyle JL, Aravanis AM, Tsien RW.** Frequency-dependent kinetics and prevalence of kiss-and-run and reuse at hippocampal synapses studied with novel quenching methods. *Neuron* 49: 243–256, 2006.
17. **Hayashi T, McMahon H, Yamasaki S, Binz T, Hata Y, Sudhof TC, Niemann H.** Synaptic vesicle membrane fusion complex: action of clostridial neurotoxins on assembly. *EMBO J* 13: 5051–5061, 1994.
18. **Holt OJ, Gallo F, Griffiths GM.** Regulating secretory lysosomes. *J Biochem* 140: 7–12, 2006.
19. **Jin S, Yi F, Zhang F, Poklis JL, Li PL.** Lysosomal targeting and trafficking of acid sphingomyelinase to lipid raft platforms in coronary endothelial cells. *Arterioscler Thromb Vasc Biol* 28: 2056–2062, 2008.
20. **Jin S, Zhang Y, Yi F, Li PL.** Critical role of lipid raft redox signaling platforms in endostatin-induced coronary endothelial dysfunction. *Arterioscler Thromb Vasc Biol* 28: 485–490, 2008.
21. **Karlsson A, Dahlgren C.** Assembly and activation of the neutrophil NADPH oxidase in granule membranes. *Antioxid Redox Signal* 4: 49–60, 2002.
22. **Lang T.** SNARE proteins and 'membrane rafts'. *J Physiol* 585: 693–698, 2007.
23. **Li N, Chen L, Yi F, Xia M, Li PL.** Salt-sensitive hypertension induced by decoy of transcription factor hypoxia-inducible factor-1alpha in the renal medulla. *Circ Res* 102: 1101–1108, 2008.
24. **Li N, Yi F, Sundy CM, Chen L, Hilliker ML, Donley DK, Muldoon DB, Li PL.** Expression and actions of HIF prolyl-4-hydroxylase in the rat kidneys. *Am J Physiol Renal Physiol* 292: F207–F216, 2007.
25. **Li PL, Zhang Y, Yi F.** Lipid raft redox signaling platforms in endothelial dysfunction. *Antioxid Redox Signal* 9: 1457–1470, 2007.
26. **Malhotra R, Valuckaite V, Staron ML, Theccanat T, D'Souza KM, Alverdy JC, Akhter SA.** High-molecular-weight polyethylene glycol protects cardiac myocytes from hypoxia- and reoxygenation-induced cell death and preserves ventricular function. *Am J Physiol Heart Circ Physiol* 300: H1733–H1742, 2011.
27. **Martin S, Tellam J, Livingstone C, Slot JW, Gould GW, James DE.** The glucose transporter (GLUT-4) and vesicle-associated membrane protein-2 (VAMP-2) are segregated from recycling endosomes in insulin-sensitive cells. *J Cell Biol* 134: 625–635, 1996.
28. **Mathay C, Poumay Y.** Lipid rafts and the oxidative stress hypothesis. *J Invest Dermatol* 130: 1457–1459, 2010.
29. **McIntosh DP, Schnitzer JE.** Caveolae require intact VAMP for targeted transport in vascular endothelium. *Am J Physiol Heart Circ Physiol* 277: H2222–H2232, 1999.
30. **McNew JA.** Regulation of SNARE-mediated membrane fusion during exocytosis. *Chem Rev* 108: 1669–1686, 2008.
31. **Mineo C, Gill GN, Anderson RG.** Regulated migration of epidermal growth factor receptor from caveolae. *J Biol Chem* 274: 30636–30643, 1999.
32. **Nevins AK, Thurmond DC.** A direct interaction between Cdc42 and vesicle-associated membrane protein 2 regulates SNARE-dependent insulin exocytosis. *J Biol Chem* 280: 1944–1952, 2005.
33. **Perrotta C, Bizzozero L, Cazzato D, Morlacchi S, Assi E, Simbari F, Zhang Y, Gulbins E, Bassi MT, Rosa P, Clementi E.** Syntaxin 4 is required for acid sphingomyelinase activity and apoptotic function. *J Biol Chem* 285: 40240–40251, 2010.
34. **Pevsner J, Hsu SC, Braun JE, Calakos N, Ting AE, Bennett MK, Scheller RH.** Specificity and regulation of a synaptic vesicle docking complex. *Neuron* 13: 353–361, 1994.
35. **Predescu SA, Predescu DN, Shimizu K, Klein IK, Malik AB.** Cholesterol-dependent syntaxin-4 and SNAP-23 clustering regulates caveolar fusion with the endothelial plasma membrane. *J Biol Chem* 280: 37130–37138, 2005.
36. **Regazzi R, Wollheim CB, Lang J, Theler JM, Rossetto O, Montecucco C, Sadoul K, Weller U, Palmer M, Thorens B.** VAMP-2 and cellubrevin are expressed in pancreatic beta-cells and are essential for Ca^{2+}-but not for GTP gamma S-induced insulin secretion. *EMBO J* 14: 2723–2730, 1995.
37. **Sarfstein R, Gorzalczany Y, Mizrahi A, Berdichevsky Y, Molshanski-Mor S, Weinbaum C, Hirshberg M, Dagher MC, Pick E.** Dual role of Rac in the assembly of NADPH oxidase, tethering to the membrane and activation of p67phox: a study based on mutagenesis of p67phox-Rac1 chimeras. *J Biol Chem* 279: 16007–16016, 2004.

38. **Shao D, Segal AW, Dekker LV.** Lipid rafts determine efficiency of NADPH oxidase activation in neutrophils. *FEBS Lett* 550: 101–106, 2003.
39. **Simons K, Ikonen E.** Functional rafts in cell membranes. *Nature* 387: 569–572, 1997.
40. **Suzuki J, Jin ZG, Meoli DF, Matoba T, Berk BC.** Cyclophilin A is secreted by a vesicular pathway in vascular smooth muscle cells. *Circ Res* 98: 811–817, 2006.
41. **Takata K, Matsuzaki T, Tajika Y.** Aquaporins: water channel proteins of the cell membrane. *Prog Histochem Cytochem* 39: 1–83, 2004.
42. **Tamori Y, Hashiramoto M, Araki S, Kamata Y, Takahashi M, Kozaki S, Kasuga M.** Cleavage of vesicle-associated membrane protein (VAMP)-2 and cellubrevin on GLUT4-containing vesicles inhibits the translocation of GLUT4 in 3T3–L1 adipocytes. *Biochem Biophys Res Commun* 220: 740–745, 1996.
43. **Tolar LA, Pallanck L.** NSF function in neurotransmitter release involves rearrangement of the SNARE complex downstream of synaptic vesicle docking. *J Neurosci* 18: 10250–10256, 1998.
44. **Touyz RM.** Lipid rafts take center stage in endothelial cell redox signaling by death receptors. *Hypertension* 47: 16–18, 2006.
45. **Varsano S, Rashkovsky L, Shapiro H, Radnay J.** Cytokines modulate expression of cell-membrane complement inhibitory proteins in human lung cancer cell lines. *Am J Respir Cell Mol Biol* 19: 522–529, 1998.
46. **Vetrivel KS, Thinakaran G.** Membrane rafts in Alzheimer's disease beta-amyloid production. *Biochim Biophys Acta* 1801: 860–867, 2010.
47. **Watson RT, Kanzaki M, Pessin JE.** Regulated membrane trafficking of the insulin-responsive glucose transporter 4 in adipocytes. *Endocr Rev* 25: 177–204, 2004.
48. **Yamakuchi M, Ferlito M, Morrell CN, Matsushita K, Fletcher CA, Cao W, Lowenstein CJ.** Exocytosis of endothelial cells is regulated by *N*-ethylmaleimide-sensitive factor. *Methods Mol Biol* 440: 203–215, 2008.
49. **Yao Y, Hong S, Zhou H, Yuan T, Zeng R, Liao K.** The differential protein and lipid compositions of noncaveolar lipid microdomains and caveolae. *Cell Res* 19: 497–506, 2009.
50. **Zhang AY, Yi F, Jin S, Xia M, Chen QZ, Gulbins E, Li PL.** Acid sphingomyelinase and its redox amplification in formation of lipid raft redox signaling platforms in endothelial cells. *Antioxid Redox Signal* 9: 817–828, 2007.
51. **Zhang AY, Yi F, Zhang G, Gulbins E, Li PL.** Lipid raft clustering and redox signaling platform formation in coronary arterial endothelial cells. *Hypertension* 47: 74–80, 2006.
52. **Zhang Z, Chen G, Zhou W, Song A, Xu T, Luo Q, Wang W, Gu XS, Duan S.** Regulated ATP release from astrocytes through lysosome exocytosis. *Nat Cell Biol* 9: 945–953, 2007.
53. **Zinchuk V, Zinchuk O, Okada T.** Experimental LPS-induced cholestasis alters subcellular distribution and affects colocalization of Mrp2 and Bsep proteins: a quantitative colocalization study. *Microsc Res Tech* 67: 65–70, 2005.
54. **Zinchuk V, Zinchuk O, Okada T.** Quantitative colocalization analysis of multicolor confocal immunofluorescence microscopy images: pushing pixels to explore biological phenomena. *Acta Histochem Cytochem* 40: 101–111, 2007.